ELSEVIER

Journal of Structural Geology 26 (2004) 1215–1230

JOURNAL OF STRUCTURAL GEOLOGY

www.elsevier.com/locate/jsg

Shear zone versus fold geometries at the Cannington Ag–Pb–Zn deposit: implications for the genesis of BHT deposits

Tony J. Roache*

School of Earth Sciences, James Cook University, Townsville, Queensland 4811, Australia

Received 10 January 2002; received in revised form 13 March 2003; accepted 6 July 2003

Abstract

Existing structural analysis of drill-core and sulphide zonation were taken as evidence for a large-scale synform that dominates the geometry of the Cannington Ag–Pb–Zn deposit—a Broken Hill-type (BHT) deposit. Underground mapping in this study has found that northwesterly directed thrusting took place during peak-temperature D_1, and that S_1 gneissosity is continuous around an amphibolite mega-boudin. D_2 sillimanite–biotite shear zones contain asymmetric folds previously interpreted to be parasitic folds, but in this study they are interpreted as due to easterly-directed extension of S_1. S_1 and S_2 indicate that shear zones were continuous and not folded into the current deposit geometry. D_2 is associated with garnet–pyroxene alteration that proved to be a favourable host for low-temperature sulphide precipitation. Retrograde deformation post-D_2 controlled lode geometry. Such a concept of high-temperature shear zone formation can be applied to other BHT deposits such as the Broken Hill Main Lode and the Aggeneys–Gamsberg base metal deposits in South Africa. In the shear zone model, Cannington and other BHT deposits are situated within high-temperature thrust shear zones that formed in conjunction with regional large-scale folding.

Keywords: Shear zones; Folds; Cannington; BHT deposits

1. Introduction

Broken Hill-type (BHT) deposits represent a small group of stratiform base metal deposits that are hosted by early-mid Proterozoic mobile belts and have undergone amphibolite to granulite facies metamorphism (Walters, 1998). Although widely thought to be metamorphosed SEDEX deposits, pre-metamorphic features are lacking in BHT deposits, and petrological, geochemical and isotopic criteria further differentiate between the two deposit types (Beeson, 1990; Parr and Plimer, 1993). Examples of BHT deposits include: Broken Hill Main Lode and Cannington, Australia; Zinkgruvan, Sweden; and Aggeneys–Gamsberg in South Africa. These deposits range in size from 30 to >250 million tonnes (Mt), and contain 10–20% Pb + Zn and >100 ppm Ag.

The origin of BHT deposits has been debated for 80 years, since detailed structural analysis started on the Broken Hill Pb–Zn–Ag deposit in western New South Wales, Australia. Geometry has been central to the argument. Early studies interpreted the current shape of mineralisation as being controlled either by pre-existing folds (Andrews, 1922; Gustafson et al., 1950; Hobbs, 1966) or by the folding of an originally stratiform ore deposit (Laing et al., 1978). Alternatively, recent interpretations of deposit fabrics have proposed high temperature shear zones as the geometric control (White et al., 1995; Rothery, 2001). The debate between a syngenetic and an epigenetic origin is heavily reliant upon geometric interpretation. The debate is important in exploration for BHT deposits, as syngenetic deposits are restricted to particular stratigraphic units, whereas epigenetic deposits may be predicted through the targeting of structural traps within areas of prospective stratigraphy.

The Cannington Ag–Pb–Zn deposit is situated off the southeast corner of the Mt Isa Inlier, Queensland, Australia (Fig. 1). The total Cannington resource as at 30th June 2001 was estimated to be 40.7 Mt at 545 g/t Ag, 12.2% Pb and 4.3% Zn, and the mine is the largest single producer of silver world-wide (Jeffrey, 2002). The Cannington deposit is hosted by Proterozoic, upper amphibolite facies quartzo-feldspathic gneiss, and lesser amphibolite and granitic pegmatite. The gneiss is considered to be part of the Maronan Supergroup (Beardsmore et al., 1988), consisting of 1.68–1.66 Ga (Page and Sun, 1998; Giles, 2000) immature siliciclastics and metabasic volcanic rocks. Peak

* Tel.: +61-7-4781-4597; fax: +61-7-4725-1501.
E-mail address: anthony.roache@jcu.edu.au (T.J. Roache).

0191-8141/$ - see front matter © 2004 Elsevier Ltd. All rights reserved.
doi:10.1016/j.jsg.2003.11.013

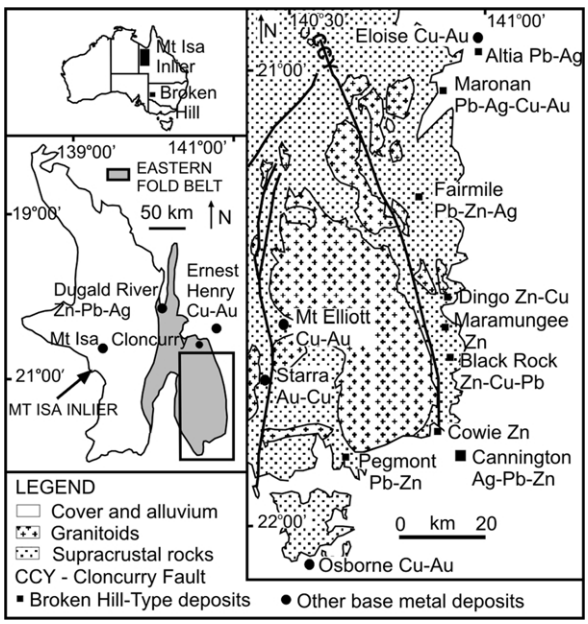

Fig. 1. Cannington Ag–Pb–Zn deposit is located off the southeastern corner of the exposed Eastern Fold Belt, Mt Isa Inlier, Australia (modified from Chapman and Williams, 1998).

metamorphic migmatitic gneiss and pegmatite have ages between 1.6 and 1.58 Ga (Giles, 2000).

Earlier structural studies at Cannington interpreted asymmetric high-temperature mineral fabrics to be parasitic folds on the limbs of large-scale folds, so that their vergence could be used to determine the position of antiformal and synformal hinges (Gray, 1992; Sheehan, 1994; Giles, 2000). Of particular note is the interpretation that a synform characterises the southern closure of a large amphibolite body, termed the Core Amphibolite. In addition to structure, repetition of zoned galena and sphalerite on either side of the Core Amphibolite give the appearance that mineralisation has been folded (Bodon, 1998; Fig. 2). The late, retrograde, NW-trending Trepell Fault divides the deposit into Northern and Southern Zones and imparts a 300 m left-lateral separation to the Core Amphibolite (Giles, 2000). Fabric orientation of the gneiss changes abruptly from the Southern to the Northern Zone, which is especially noticeable at the northern end of the Core Amphibolite. A N-trending open fold is interpreted to deform peak-metamorphic fabrics and the Core Amphibolite at this northern closure (Gray, 1992; Giles, 2000). The Hamilton Fault passes tens of metres to the south of the southern Core Amphibolite closure, and is considered to be similar to, but smaller than the Trepell Fault.

Several metasomatic events have been identified at Cannington, ranging from high-temperature skarn-like garnet–pyroxene alteration, to low-temperature chlorite–carbonate fault-related brecciation. Textural interpretation of the timing of sulphide introduction is inconsistent. Bodon (1998) proposes that sulphide was stable at all stages, including pre-metamorphic, whereas Chapman and Williams (1998) observe sulphide to be associated only with the Trepell and Hamilton Faults. It is clear that the bulk of sulphide at Cannington has crystallised as a retrogressive phase, whether the current lode geometries are indicative of pre-metamorphic mineralised horizons or not. Indeed, the greatest concentration of mineralisation is where sulphide is parallel to late faulting and discordant to the early layering. Hence, sulphide textures in this study are described as retrograde, since they all overprint the high-temperature fabrics. These include the ore minerals sphalerite and galena, as well as arsenopyrite, chalcopyrite and pyrrhotite. The Trepell and Hamilton Fault systems have been described as responsible for the introduction of silver (Bodon, 1998; Chapman and Williams, 1998), and, as silver has an overriding economic significance, such faulting is important in the development of a minable resource.

In order to clarify the geometry of BHT deposits, this study at Cannington involved a reassessment of the geometry of high-temperature fabrics that combined underground exposure, oriented hand sample and thin section observation, and stereographic projection of structural data. Microscopic mineral textures and geometry were used in the first stage of interpreting the mineral paragenesis. Chemical analysis of garnet in association with mineral texture enabled interpretation of fabrics across host rock and alteration transitions, as garnet is common to all high-temperature mineral assemblages. Finally, a consideration of metasomatism and a review of deposit- and regional-scale geometry, contribute to the discussion of whether shear zones or folds are responsible for the geometry of Cannington and some other BHT deposits.

2. Cannington geometry

Two major, penetrative deformation events (D_1 and D_2) can be distinguished at Cannington. These deformation events define high temperature mineral fabrics in gneiss, pegmatite and amphibolite that have been dated as peak metamorphic (Giles, 2000).

2.1. D_1

K-feldspar–quartz–biotite–garnet gneissosity (S_1) is the main fabric that defines the earliest recognized phase of mineral growth. Structural data from underground mapping reveal that S_1 strikes N–NE, has a moderate to steep easterly-dip, and continues past the southern closure of the Core Amphibolite (Fig. 3). S_1 is consistent in its intensity throughout the Southern Zone, an approximate volume of 500 m^3 that is delineated by underground workings. S_1 is not developed within the Core Amphibolite except at its margins and in small amphibolite bodies within the surrounding gneiss (Fig. 4). The amphibolite is altered to biotite–garnet (–ilmenite) schist and plagioclase–quartz leucosomes that are concordant with the adjacent gneiss.

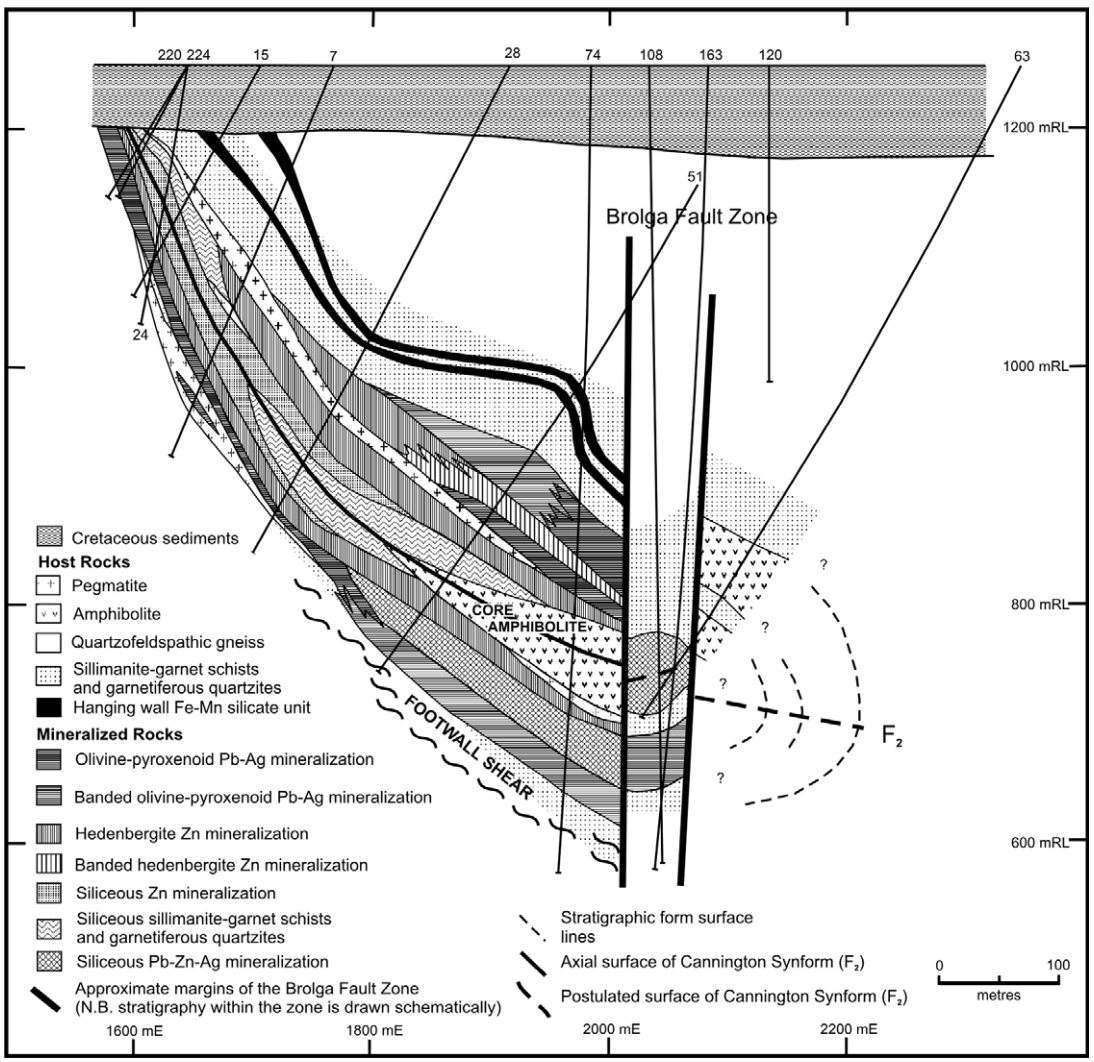

Fig. 2. Interpretive geological cross-section 4700 mN of the Southern zone, with F_2 closure (from Bodon, 1998).

Plagioclase–quartz leucosomes along altered amphibolite margins grade into K-feldspar–quartz within the gneiss. The biotite–garnet schist preserves a biotite mineral elongation lineation (L_1) that varies in orientation from an ESE to SSE plunge.

K-feldspar–quartz pegmatite bodies, up to tens of metres in width, have margins that are concordant with the surrounding gneiss, and locally have garnet banding concentrated at their margins. Garnet banding is texturally associated with K-feldspar and quartz, and parallel to aplitic and biotite-foliated margins (Fig. 5). Synchroneity between pegmatite crystallisation and biotite growth is implied by the intrusion of a discordant lens of aplite into the marginal biotite foliation. The aplite has been subsequently folded during progressive development of the biotite foliation (Fig. 5).

D_1 garnet is texturally diverse, with grain sizes from less than a millimetre to 3 cm and aggregates of fine-grained garnet that have a planar to spheroidal shape. There is a sequential increase in grain size through pegmatite, gneiss and biotite–garnet schist. The garnet is an unzoned almandine that displays minor changes in its chemistry between rock types. Electron microprobe analyses show that the MgO content of garnet within pegmatite and gneiss increases in biotite–garnet schist, which is matched by a two-fold MgO increase in biotite from gneiss to schist (Table 1). Changes in garnet and biotite chemistry occur together with changes in host rock chemistry, which in combination with textural observation assist in determining the relation of garnet banding, gneissosity and biotite–garnet schistosity.

Sections perpendicular to S_1 and parallel to L_1, or vertical SE-trending sections when L_1 is absent, show S_1 asymmetries within pegmatite, gneiss and biotite–garnet schist. Deformed pegmatite margins (Fig. 5) can be interpreted to have a fold vergence of top-to-the-WNW. Biotite–garnet melanosomes within gneiss, in conjunction with a σ-clast comprised of texturally and chemically compatible quartz–garnet, indicates a top-to-the-NW shear sense (Fig. 6a). Biotite asymmetry around garnet suggests a

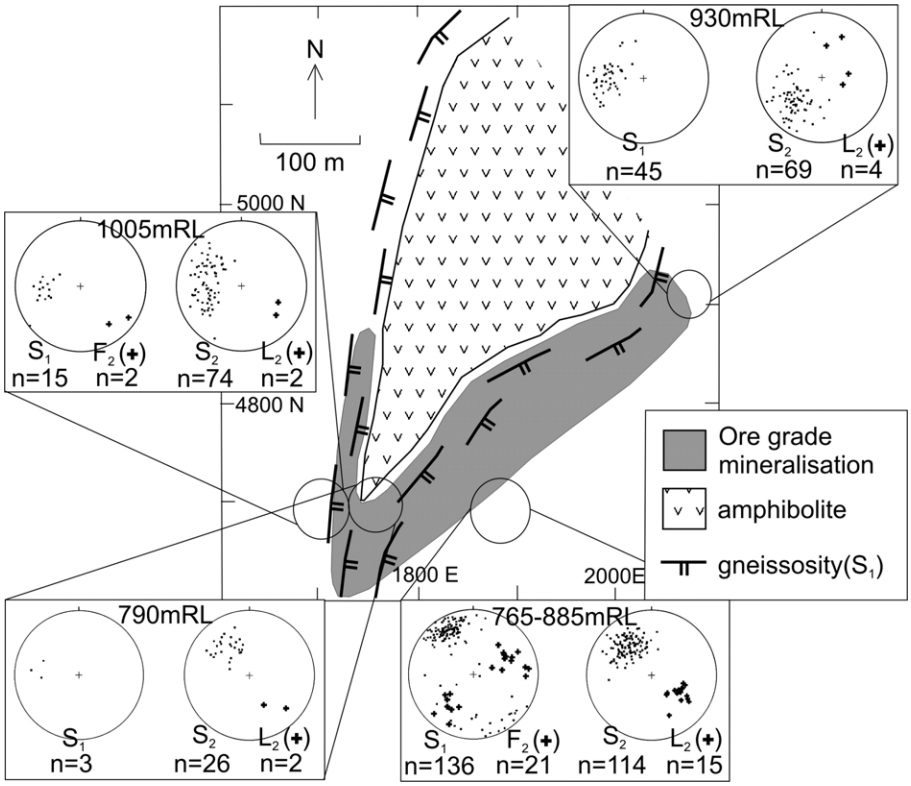

Fig. 3. Plan of the southern end of the core amphibolite at 940 mRL, with a schematic outline of economic mineralisation and anastomosing S_1. The outline of the Core Amphibolite is derived from underground mapping and drill core, and the orientation of S_1 from underground mapping. Coordinates are the local mine grid. Poles to S_1 and S_2, L_2 and F_2 are plotted on lower hemisphere equal area stereographic projections, and are from different mine levels.

Fig. 4. Amphibolite (outlined) is concordant with the surrounding quartzofeldspathic gneiss (4460 mN, 1821 mE, 887 mRL). Leucosomes range from plagioclase-rich at amphibolite margins (light), to K-feldspar-quartz (dark) within the gneiss. A late fault displaces the amphibolite and gneiss. Hammer for scale.

top-to-the-WNW shear sense and is compatible with anticlockwise rotation of garnet (cf. Passchier et al., 1992), based on the asymmetry of quartz inclusion trails (Fig. 6b). Variation in shear sense between WNW and NNW is associated with the variation in L_1 orientation. S_1 encloses the Core Amphibolite and the rock fabric shows a top-to-the-NW sense of shear.

2.2. D_2

S_2 is defined by the orientation of intergrown biotite and sillimanite, and overprints and deforms S_1. Biotite–sillimanite mineral elongation (L_2) is measurable in outcrop, and was also observed through its preferred elongation in oriented slabs and thin-sections. The orientation of S_2 and L_2 varies over the deposit. In areas of N-striking S_1, S_2 has an average NW strike and a moderate to steep dip, and L_2 on average plunges to the NE. In areas of NE-striking S_1, S_2 has an average NE strike and a moderate to steep dip, and L_2 on average plunges to the SE (Fig. 3). Deformed S_1 leucosomes delineate measurable fold axes (F_2) that were predominately observed in the SE part of the mine, where observation was assisted by better quality exposure. SE-trending, shallowly-plunging F_2 were measured where NW-striking S_2 intersects N-striking S_1 (Fig. 3). Where S_2 is approximately parallel to the orientation of S_1 in the SE corner of the deposit, F_2 has two main orientations. Change in the orientation of F_2 is

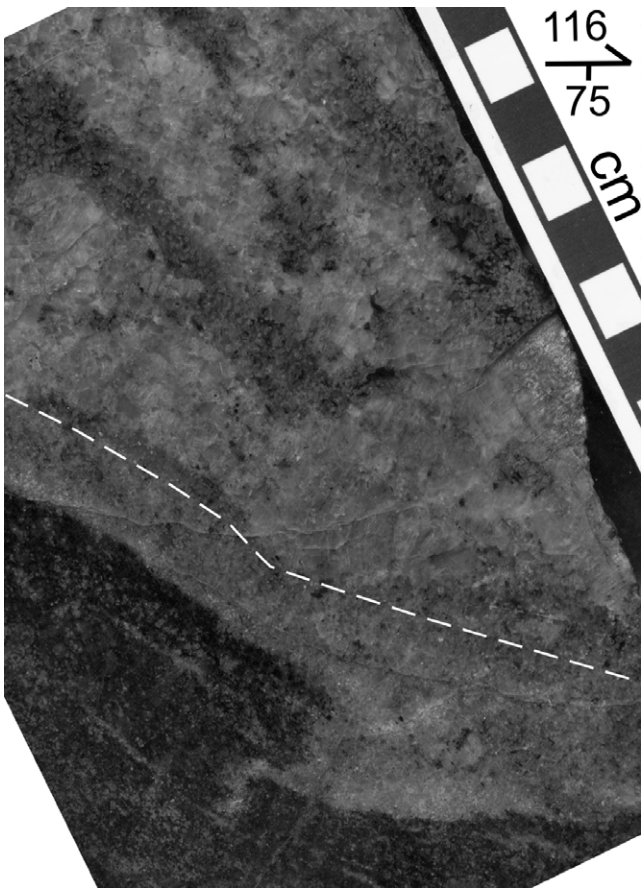

Fig. 5. Polished slab showing garnet banding that is parallel to a pegmatite contact and biotite foliation (4892 mN, 2027 mE, 930 mRL). Aplite along the pegmatite margin is locally discordant with the adjacent biotite foliation, but is also folded into parallelism with the biotite foliation (bottom centre). The dashed line represents the boundary between pegmatite and aplite.

spatially related to a variation in the strike of S_2. S_2 generally has a shallower dip than S_1, but the strike of S_2 may vary from a more southerly orientation than S_1 (SW-plunging S_1/S_2 intersection), to a more easterly orientation than S_1 (NE-plunging S_1/S_2 intersection), as shown in Fig. 7a and b, respectively. Although a single exposure predominantly contains either NE- or SW-plunging F_2, changes in F_2 orientation on the metre scale are also associated with a localised change in S_1/S_2 intersection orientation (Fig. 7a).

S_2 forms up to 10-m-wide pervasive shear zones throughout the host gneiss, but is otherwise intermittently distributed. S_2 forms parallel to S_1 leucosomes, but also develops at an oblique angle to S_1. Both orientations of S_2 are associated with the distortion of S_1, but the cross-cutting orientation is associated with most of the folding and measurable F_2 (Fig. 8a). When sectioned parallel to L_2, deformed leucosomes and asymmetries of folded biotite and sillimanite are seen to have a consistent top-to-the-E vergence or a normal shear sense, which is opposite to the thrust shear sense of S_1. Asymmetries are relatively uncommon in areas of minor S_2 development (Fig. 8a), but increase in frequency with intensification of S_2 (Fig. 8b). Sillimanite is the only mineral that develops within leucosomes and pegmatite, where its presence mimics the larger-scale geometry (Fig. 8c).

F_2 shape and attitude increase in irregularity towards zones of undeformed pegmatite, and although muscovite does not form a planar fabric, the discordance of the muscovite-rich pegmatite to deformed S_1 suggests an origin syn- to post-D_2 (Fig. 7a). K-feldspar–quartz leucosomes are frequently at an oblique angle to the dominant S_1 orientation and parallel to cross-cutting S_2 (Fig. 8a). These D_2 fabrics are texturally associated with garnet (Fig. 8b) that is chemically distinct from S_1-related almandine, but texturally similar to grossular garnet related to pyroxene alteration around the Core Amphibolite. D_1 almandine within biotite schist may have up to 5% CaO, but consistently has 30–35% FeO/Fe_2O_3, whereas grossular-rich garnet ranges from 10 to 22% CaO and 10 to 24% FeO/Fe_2O_3 (Table 2). There is a diverse chemistry of grossular-rich garnet that appears to be related to the bulk rock chemistry, therefore mapping and textural observation have been used to correlate the genesis of these garnets across chemical transitions. Usually, garnet–pyroxene alteration is homogeneous, but metre-wide zones of aligned pyroxene (hedenbergite) and garnet are macroscopically delineated by the precipitation of sulphide. There are sharp transitions from aligned hedenbergite–garnet to similarly-oriented biotite–sillimanite schistosity along strike (Fig. 9), which in combination with garnet texture, suggests that grossular-rich garnet and pyroxene are a D_2 assemblage.

Mineral textures of ambiguous timing are characteristic of obliquely-intersecting S_2, where multiply-oriented biotite and sillimanite have been deformed and recrystallised. Porphyroblastic muscovite predominantly overgrew intergrown biotite–sillimanite, but in places is overgrown by fine-grained prismatic sillimanite. Relative timing between muscovite and biotite–sillimanite growth becomes clearer when combined with a consideration of S_2 geometry. Kink-bands increase in number with intensification of S_2, which is similar to the habit of multiply-oriented S_2 (Fig. 8a). Kink-bands have also nucleated from the edges of leucosomes and radiate in minor fans into the surrounding biotite–sillimanite–muscovite matrix, which is characteristic of S_2 (Fig. 10). The kink bands are associated with S_2, but unlike other S_2, the biotite, sillimanite and muscovite have undergone solid-state deformation within the kink bands, rather than being recrystallised. The last criterion, in conjunction with the syn- to post-growth of muscovite in relation to sillimanite, implies that the kink bands and muscovite formed late in D_2.

2.3. The Cannington synform—fact or fiction?

Several inadequacies exist in the interpretation that leucosome and biotite–sillimanite asymmetric folds are

Table 1
The chemistry and calculated end-members of D_1 garnets. Garnet chemistry is controlled by the bulk chemistry of the host rock and individual garnets are essentially unzoned

Rock type	Pegmatite		Gneiss			Biotite schist		
Mineral	Garnet		Garnet		Biotite	Garnet		Biotite
	Rim	Core	Rim	Core		Rim	Core	
SiO_2	37.48	37.31	36.84	37.84	33.12	37.72	37.57	34.77
TiO_2	0.08	0.11	0.03	0.00	2.58	0.03	0.08	2.13
Al_2O_3	20.82	21.25	21.38	20.96	17.21	20.15	20.08	15.09
FeO/Fe_2O_3	29.64	31.36	33.73	33.05	27.32	30.21	31.98	23.44
MnO	6.25	5.48	3.22	4.27	0.26	3.20	1.42	0.18
MgO	0.66	0.83	0.78	0.89	3.54	1.92	2.39	7.89
CaO	3.70	3.10	2.84	2.87	0.21	5.73	5.31	0.05
Na_2O	0.19	0.03	0.00	0.13	0.21	0.03	0.08	0.22
K_2O	0.06	0.04	0.12	0.00	8.43	0.05	0.03	8.27
Cl	0.01	0.03	0.04	0.04	0.49	0.00	0.07	0.32
Total	98.88	99.52	98.98	100.05	93.27	99.05	99.01	92.29
Mol.% garnet end-members								
Pyrope	2.81	3.48	3.31	3.72		7.74	9.59	
Almandine	70.77	74.04	80.27	77.52		68.31	71.88	
Spessartine	15.11	13.11	7.77	10.13		7.34	3.24	
Grossular	11.31	9.37	8.65	8.62		16.61	15.29	
Total	100.00	100.00	100.00	100.00		100.00	100.00	

parasitic to large-scale folds. The first is that the vergence of parasitic folds on individual limbs is not consistent with this interpretation. Earlier structural studies (Gray, 1992; Sheehan, 1994; Giles, 2000) were based on predominately unorientated diamond drill core and did not have the benefit of subsequent detailed paragenetic work (Richmond et al., 1996; Chapman and Williams, 1998; Mark et al., 1998). Bodon (1998) has attempted to incorporate the early structural interpretation to the paragenesis of the mineralised zone, and asserted that the current geometry is controlled by the folding of a pre-existing stratiform ore deposit and genetically associated mafic volcanic protolith (Gray, 1992; Sheehan, 1994; Walters and Bailey, 1998). Much of the reasoning behind the synform scenario is based on interpretation of the current geometry of the Core Amphibolite and mineralisation. With increasing infor-

Table 2
The chemistry and calculated end-members of D_2 garnets. Garnet chemistry is controlled by the bulk chemistry of the host rock and individual garnets are essentially unzoned

Alteration type	Quartz–garnet veining in amphibolite/biotite schist		Quartz–garnet veining in gneiss		Pyroxene (hedenbergite) –garnet		
Mineral	Garnet		Garnet		Garnet		Hedenbergite
	Rim	Core	Rim	Core	Rim	Core	
SiO_2	38.00	37.73	37.75	37.56	37.12	36.94	48.12
TiO_2	0.04	0.07	0.04	0.26	0.09	0.00	0.02
Al_2O_3	19.06	18.59	20.92	20.76	18.82	18.41	0.00
FeO/Fe_2O_3	24.59	21.91	12.45	12.33	22.93	24.54	26.27
MnO	2.38	3.63	8.38	6.88	8.96	7.56	2.09
MgO	0.56	0.56	0.37	0.19	0.24	0.20	0.84
CaO	16.90	16.42	19.87	21.49	10.55	11.63	21.55
Na_2O	0.00	0.08	0.15	0.00	0.07	0.24	0.56
K_2O	0.00	0.02	0.02	0.06	0.05	0.00	0.00
Cl	0.04	0.03	0.06	0.07	0.04	0.04	0.03
Total	101.57	99.01	100.01	99.59	98.83	99.54	99.45
Mol.% garnet end-members							
Pyrope	2.02	2.08	1.41	0.72	0.91	0.75	
Almandine	49.52	46.01	26.45	26.14	49.91	51.72	
Spessartine	4.85	7.72	18.04	14.78	19.76	16.14	
Grossular	43.61	44.19	54.10	58.36	29.42	31.39	
Total	100.00	100.00	100.00	100.00	100.00	100.00	

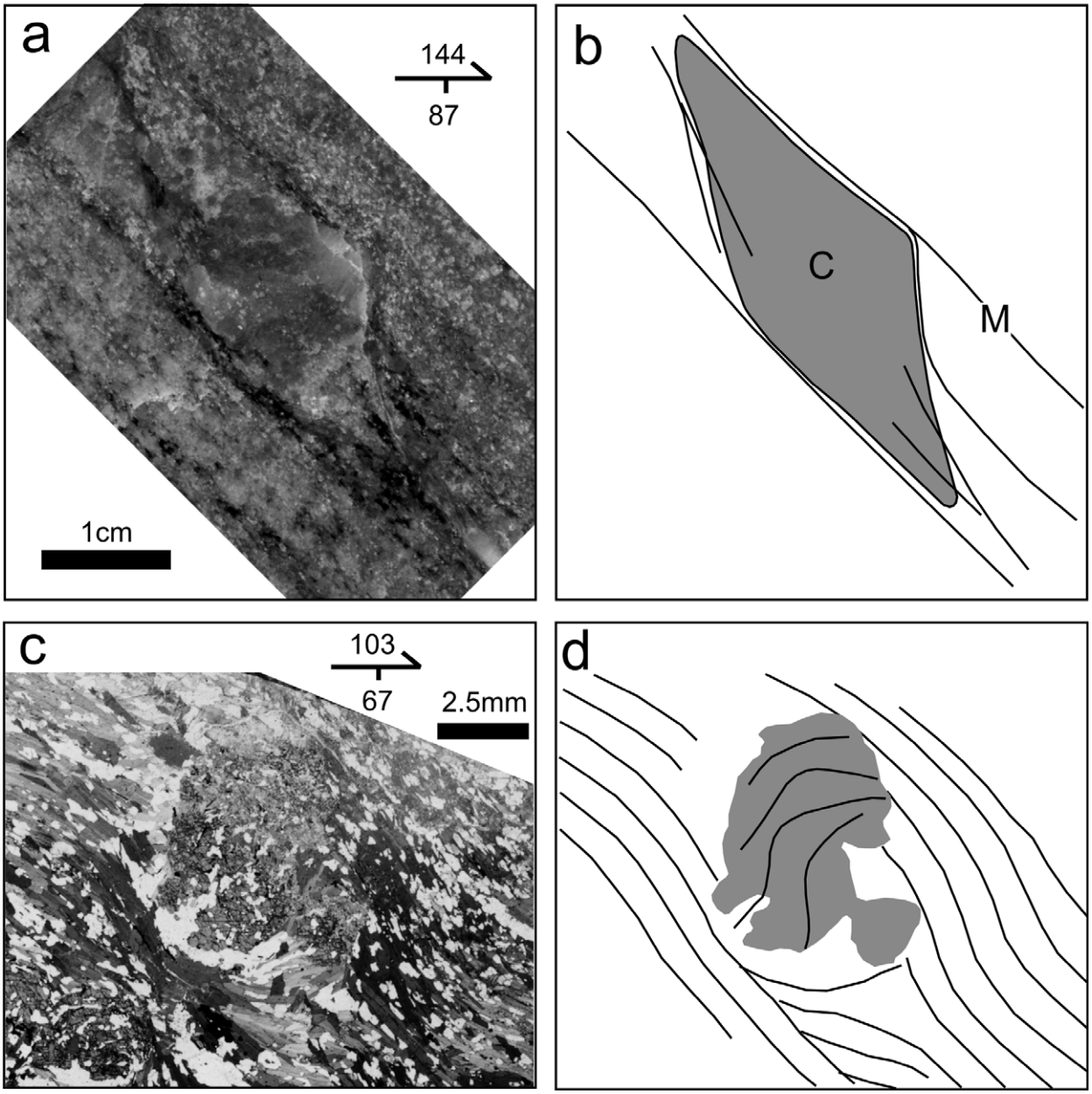

Fig. 6. S_1 asymmetries indicating a top-to-the-NW shear sense. (a) Photograph of gneiss showing biotite–garnet melanosomes (M) that wrap around a sigmoidal garnet–quartz clast (C). (b) Line diagram of (a). (c) Photomacrograph in plane polarised light of biotite–quartz asymmetry around garnet within biotite schist. (d) Line diagram of (c).

mation from drilling and development, the deposit geological model continues to suggest a 'folded' geometry much like Fig. 11a (pers. comm., A. Edwards, 2002). Documentation of fabrics in this study show that large-scale folding did not take place at the time of peak-temperature deformation, but that retrograde deformation (e.g. open folding in the Northern Zone; Giles, 2000) modified the high-temperature geometry.

The consistent vergence of S_1 asymmetries in small-scale structures either side of the Core Amphibolite suggests that Cannington was situated in a thrust shear zone with a top-to-the-NW sense of shear during D_1. S_1 defines the outline of the Core Amphibolite, a mega-boudin, and is interpreted to reflect an asymmetry that is compatible with small-scale structures (Fig. 11b), before retrograde deformation of S_1/S_2 as outlined above. Previous study (Giles, 2000) has suggested the existence of shear zones during D_2. Intergrown biotite–sillimanite has been attributed to the formation of metasomatic shear zones that are associated with fluid derived from partial melting. D_2 metasomatism has been used to explain the repetition of pyroxene–garnet alteration assemblages either side of the Core Amphibolite (Chapman and Williams, 1998), which has also been interpreted as a structural repetition of mineralised strata (Gray, 1992; Walters and Bailey, 1998). High-temperature metasomatism between external fluid/s and

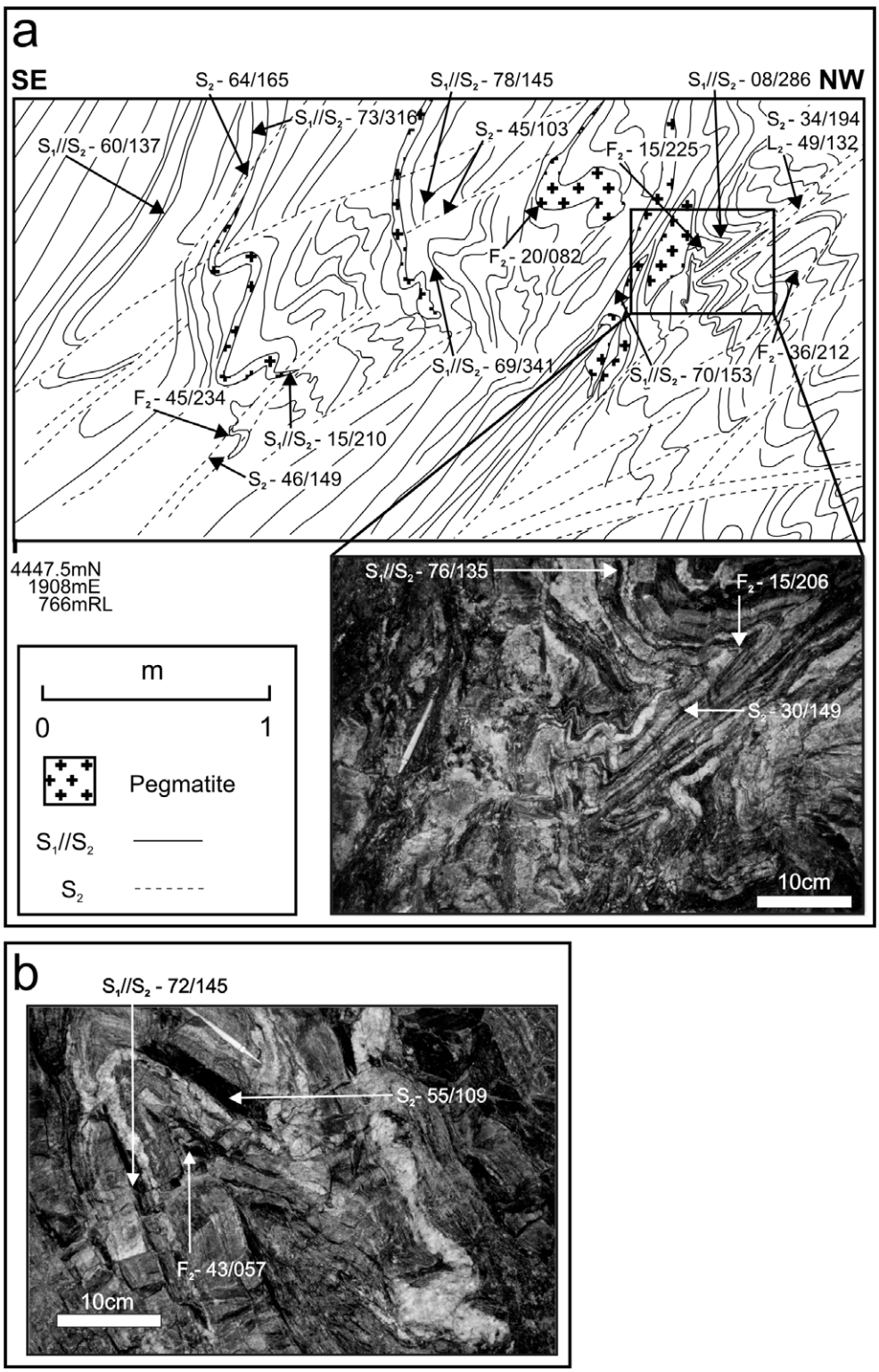

Fig. 7. S_2 asymmetries in the SE corner of the deposit, with planes and lineations as dip/dip-direction and plunge/trend, respectively. (a) Underground wall mapping (4447.5 mN, 1908 mE, 766 mRL) showing a consistent sense of asymmetry where S_2 obliquely intersects S_1/S_2 when viewed in a section parallel to the dominant SE-plunging L_2. Mainly SW-plunging F_2 forms in this exposure. A localised variation in fold shape and attitude is due to an increasing melt fraction to the left of the photograph, and ultimately the crystallisation of a muscovite-rich pegmatite that replaced the gneissic layering. (b) Photograph looking to the east at another exposure (4439 mN, 1825 mE, 888 mRL), showing dominant NE-plunging F_2.

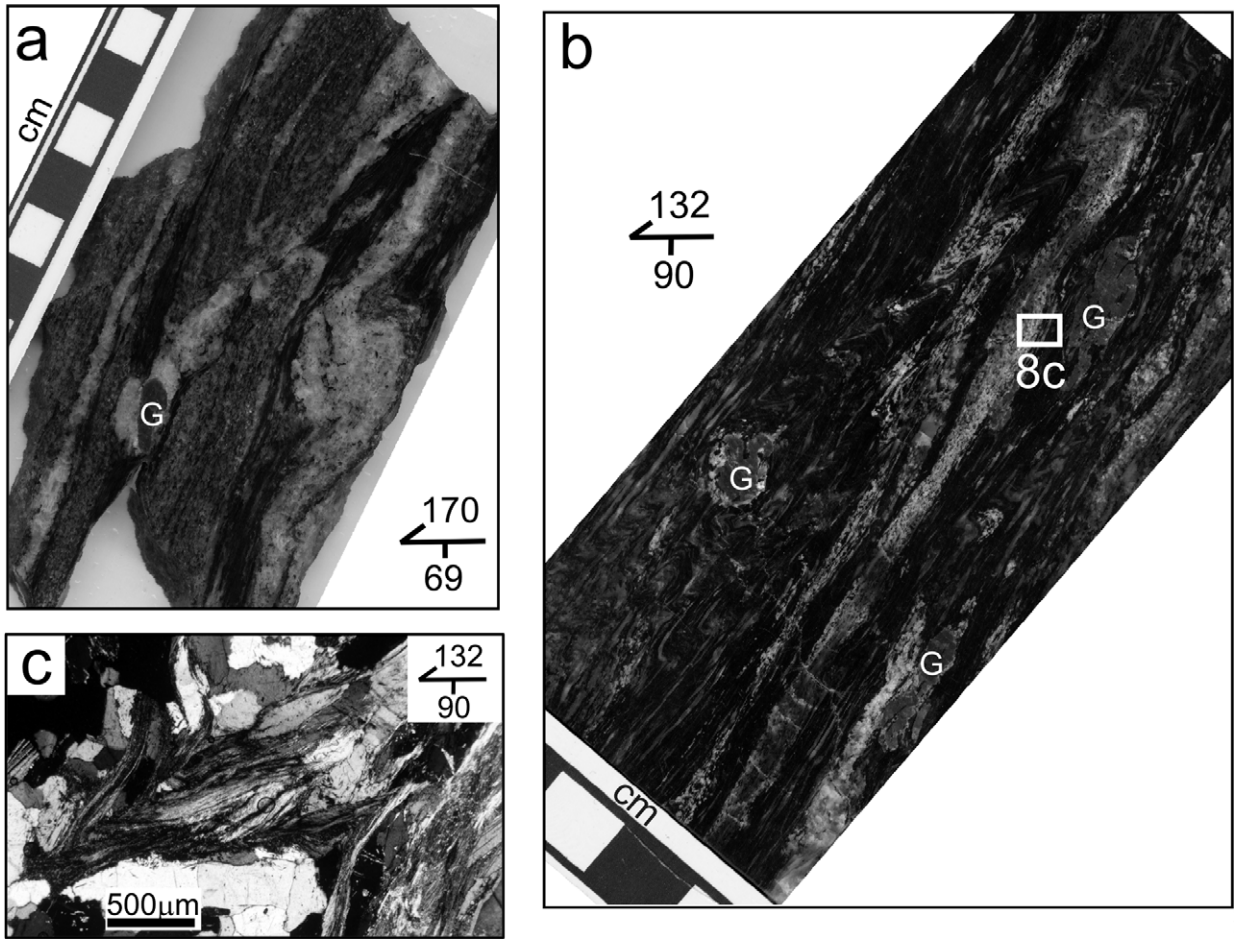

Fig. 8. Small-scale S_2 asymmetries. (a) Polished slab oriented perpendicular to S_1/S_2 and parallel to L_2. Development of S_2 oblique to the main S_1 orientation is uncommon outside of areas greatly affected by D_2. The folded, wider leucosome on the right has a fold axis approximately perpendicular to L_2, and is non-cylindrical in form. Interpreted rotation of S_1 in a down-dip direction conforms to the displacement sense of folded leucosomes by obliquely-oriented S_2. Grossular-rich garnet (G) and K-feldspar–quartz leucosome are concordant with S_2. (b) Polished slab oriented perpendicular to S_1/S_2 and parallel to L_2. Leucosome folding increases in frequency towards the centre of the most intense biotite–sillimanite shear zones. Grossular rich garnet (G) is concordant with the main S_2 orientation, and is also seen within oblique S_2. (c) Photomicrograph under cross-polarised light of sillimanite mimicking the asymmetry of deformed S_1.

the Core Amphibolite could explain the proximal Fe-rich, hedenbergite-dominated zone, and the distal Mn-rich, pyroxmangite-dominated zone. Sphalerite and galena selectively overprinted the hedenbergite and pyroxmangite zones, respectively, during retrograde metasomatism. Metre-scale amphibolite bodies that mimic the sulphide zoning of the Core Amphibolite have been identified by mine geologists in diamond drill-core tens of metres into the footwall gneiss (pers. comm., T. Kennedy, 2002). These bodies may be a small-scale representation of the Core Amphibolite, and strongly support a metasomatic-origin for mineralisation, rather than large-scale folding of a pre-existing deposit. Furthermore, parallel S_1 almandine banding and pyroxene–garnet S_2 that are continuous past the southern closure of the Core Amphibolite demonstrate that neither fabric delineates a fold closure. In combination with consistent S_1 and S_2 asymmetries either side of the Core Amphibolite, it is suggested that folding could only have taken place during prograde deformation (pre-D_1), and any evidence for this has subsequently been removed through migmatisation. Hence, it is not likely that sulphide distribution around the core amphibolite was caused by the folding of a pre-existing stratiform ore deposit, but was preferentially deposited upon S_1/S_2 during a lower-temperature retrograde event.

2.4. Shear zone geometry and microstructure

Giles (2000) interpreted two generations of sillimanite growth based on a change in mineral orientation, and that biotite–sillimanite folds are parasitic to large-scale folding, whereas in this study shear zone deformation is shown to be compatible with a single protracted stage of sillimanite growth during D_2. On the deposit-scale, change in S_2 orientation is caused by cleavage refraction within areas of differently oriented S_1, but on the small-scale sillimanite and biotite were deformed and rotated within the shear zone, with continued mineral growth during D_2 obscuring

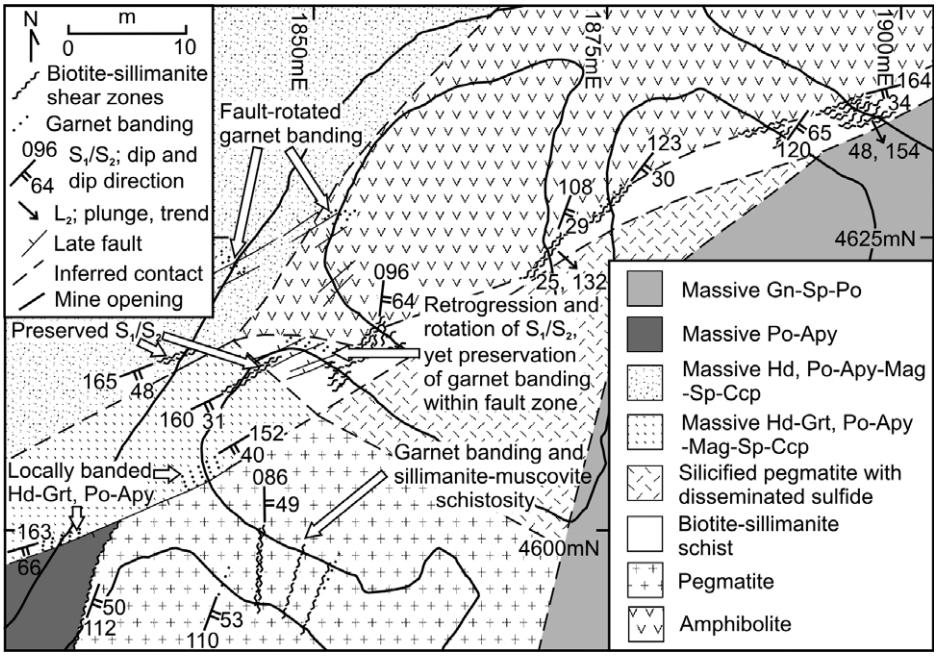

Fig. 9. Plan view of underground mapping at the southern closure of the core amphibolite (790 mRL). S_1 and S_2, represented by garnet banding and biotite–sillimanite schistosity, respectively, are preserved within a linear zone adjacent to the SE amphibolite contact. Continuing along the above trend beyond the closure of the Core Amphibolite is a zone of hedenbergite (Hd)–garnet (Grt), which is distinct from the adjacent areas that contain no garnet intergrown with hedenbergite. Within the Hd–Grt zone, localized garnet banding is parallel to the pegmatite contact, with later fault reactivation and sulphide overgrowth of the original fabric. The influence of the Core Amphibolite on the orientation is apparent in the transition between dominantly NE–SW- to N–S-trending S_1 and S_2 from north to south. Late, localized fault rotation of S_1 and S_2 is always associated with the obliteration of biotite and sillimanite yet marked by relic garnet banding. Pyrrhotite (Po), arsenopyrite (Apy), magnetite (Mag), sphalerite (Sp), galena (Gn) and chalcopyrite (Ccp) have preferentially grown parallel to the garnet banding within the rotated fault blocks.

solid-state deformation. Shear zone asymmetries are associated with passive rotation parallel to S_1, combined with active folding in an oblique orientation to S_1 (Fig. 12). An increase in active folding and a wider variation of S_2 orientation is related to an increase in shear zone intensity and anisotropy between leucosomes and schistosity, which is comparable with a situation of internal instability (cf. Cobbold et al., 1971). The normal shear sense of D_2 fabrics implies that extension replaced compression after thrust shear zone formation. The change from compression during D_1, to extension of S_1 during D_2, is temporally related to the onset of D_2 metasomatism, which may have been driven by fluid derived from crystallising melt (cf. Mark et al., 1998). Therefore, it is suggested that biotite–sillimanite shear zones acted as conduits for fluid that precipitated garnet–pyroxene in low strain zones of extended S_1. D_2 shear is also responsible for the folds previously interpreted (Gray, 1992; Giles, 2000) as parasitic to coaxial folding.

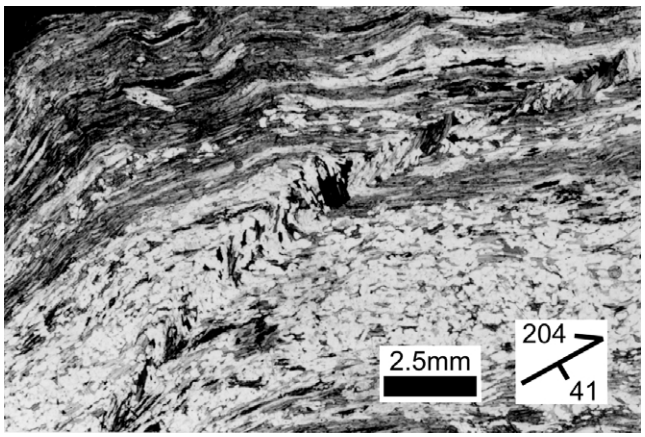

Fig. 10. Photomacrograph in a field of view approximately perpendicular to L_2, from the same specimen as in Fig. 8b, showing S_2 kink-bands within interlayered biotite–sillimanite–muscovite schistosity that radiate from leucosome margins (top right field of view). S_2 that has an orientation oblique to S_1 is in spatial affinity with the kink bands and deformed leucosomes, but its obliquity gradually diminishes into the surrounding schistosity along strike.

Proto-sheath folding may account for the D_2 folds that have a top to the east vergence sub-parallel to L_2, yet have multiple F_2 orientations, especially as there is no evidence of multiple mineral elongation lineations or cleavages that would suggest refolding. F_2 and L_2 plot along a common great circle girdle that represents the S_2 shear plane, therefore the shear strain involved in rotating F_2 towards the direction of shear, L_2, may be calculated (Fig. 13a). The intersection of the initial marker, S_1, and the shear zone, S_2, form a line making an angle α with the direction of shear (Fig. 13b). In this study the maximum α is taken to be 90°, but a line with any value of α may be deformed to angle α',

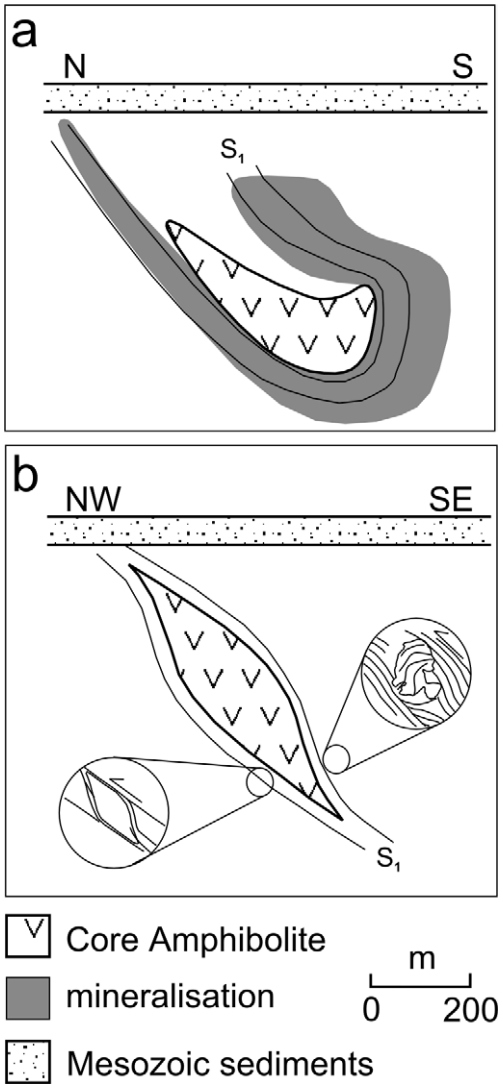

Fig. 11. Schematic diagrams of the interpreted deposit-scale geometry at Cannington. (a) N–S section showing the Core Amphibolite interpreted as a synformal hinge that folded pre-existing high-temperature fabrics and mineralisation (modified after Giles (2000)). (b) NW–SE section showing the high-temperature shear zone geometry that is interpreted in this study, prior to retrograde deformation and mineralisation. Section is in a plane parallel to L_1, highlighted by the consistent vergence of S_1 asymmetries either side of the Core Amphibolite.

thus enabling a calculation of the shear strain, γ:

$$\cot\alpha' = \cot\alpha - \gamma$$

(Ramsay and Graham, 1970, eq. 37).

Direct measurement of the acute angle ψ is used to find α' (Fig. 13b):

$$\alpha' = 180° - \psi$$

The scatter of F_2 orientations along the shear plane signifies intensification of the shear strain towards L_2, and from the selected outcrops maximum and minimum estimates have been calculated. The minimum estimated value of γ is 0.9, where $\psi = 48°$, and is due to an observable

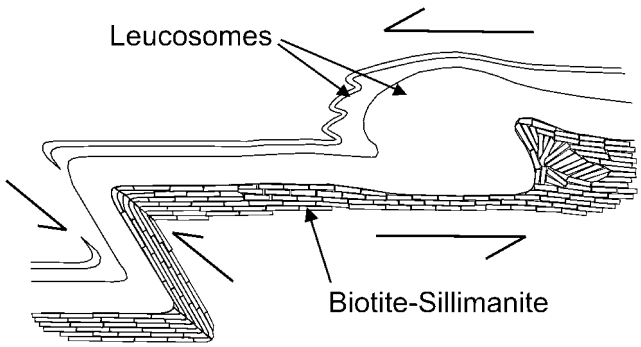

Fig. 12. Schematic diagram showing a similar asymmetry between deformed S_1 and S_2 mineral growth. The fold symmetry of S_1 implies a bulk sinistral shear sense of movement of leucosome-parallel S_2 in this plane of view (right). The gradual change in orientation of mineral growth within deformed leucosome 'strain shadows' implies growth during the rotation of S_1. Subordinate shear zone development via internal instability indicates a synthetic shear sense to that of bulk leucosome-parallel shearing by means of drag-folding of S_1 and S_2, and the continued growth of biotite and sillimanite to recrystallise the hinges and obscure solid-state deformation (left).

low intensity of S_2 where predominantly SW-plunging F_2 was measured. The maximum estimated value of γ is 2.5, where $\psi = 22°$, which is associated with an intense, 10 m-wide D_2 shear zone. Note that both of these shear strain measurements represent a minimum value, since the proportion of strain from shear zone formation to fold initiation is not possible to record. Nevertheless, in conjunction with field observation, the shear strain determined by this method is useful in relating the geometry of D_2 fabrics to shear zones. F_2 reflect the change in fold hinge-line vergence (FHLV) either side of sheath fold culminations/depressions (cf. Alsop and Holdsworth, 1999). The change in F_2 orientation is related to the scale at which the sheath folds form. At the scale of mapped exposures, a single dominant F_2 orientation is a reflection of the FHLV on one limb of a major culmination/depression. Minor recording of the other F_2 orientation in a single exposure reflects a change in FHLV on the centimetre- to metre-scale, which is related to the spacing of secondary culminations/depressions.

Analysis of multiple fold generations in high temperature terranes is complicated by the presence of melt during deformation, which locally affects fold geometry. An increasing melt fraction means that deformation approaches magmatic flow and therefore reduces the influence of tectonic stresses (McLellan, 1984, 1988). As a result, the interpretation of irregular fold interference patterns as the refolding of multiple fold generations is complex, especially as there is an observable correlation between increasing melt fraction and fold irregularity (Fig. 7). Fig. 7 also has implications for the progression of deformation from D_1 to D_2 at Cannington. Partial melts display a transition from solid state deformation to magmatic rupture of the migmatitic layering, which suggests that either the deformation was still close to magmatic or another phase of

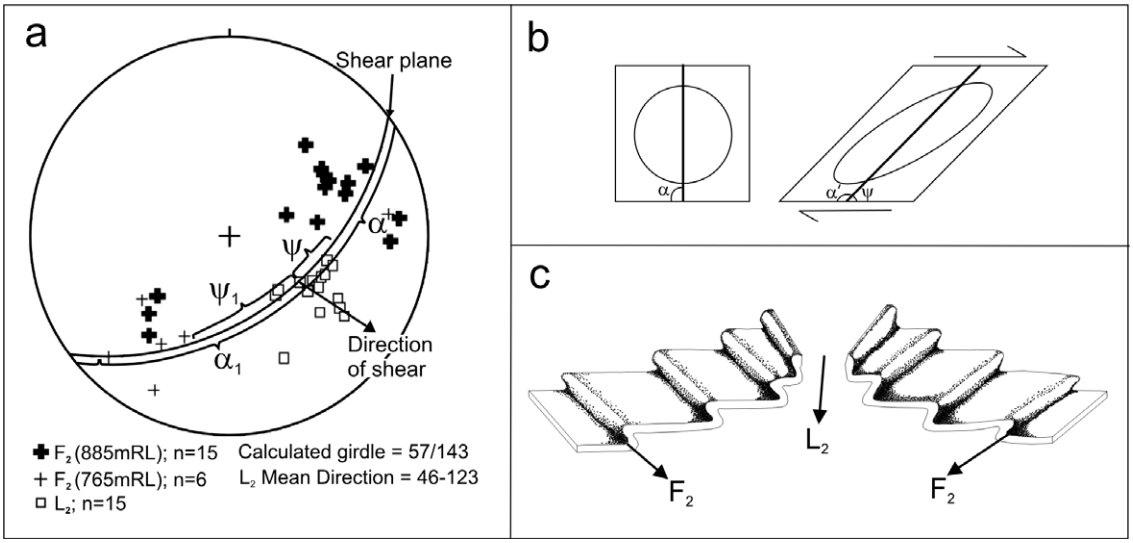

Fig. 13. Proto-sheath fold geometry. (a) Lower hemisphere, equal area stereographic projection of F_2 collected from two locations in the SE corner of the deposit. All measurements cluster around a great circle girdle that represents the S_2 shear plane, with the mean L_2 orientation representing the direction of shear. (b) Prior to D_2, the linear intersection between S_1 and the shear zone, termed the linear marker, makes an angle α with the direction of shear, denoted as 90°. Shearing involves the rotation and folding of S_1 in the direction of shear. The final strained state of the deformed linear marker is taken as the angle α', or directly measured off the stereographic projection as the acute angle ψ. The spread of F_2 along the shear plane represents the deformed linear marker and varying degrees of shear strain. (c) Schematic diagram showing the geometry of folding. F_2 orientations may change substantially between exposures, with a predominance of either SW- (765 mRL; Fig. 7a) or NE-plunging folds (885 mRL; Fig. 7b) in any one location, in relation to the direction of L_2 (modified from Alsop and Holdsworth (2002)).

melting took place during D_2. In either case, D_1/D_2 had an episodic and heterogeneously distributed melting and cooling history. Crystallisation of coarse muscovite-rich pegmatite is a reflection of lowering melt temperature in the last stages of D_2.

3. BHT deposits and regional-scale deformation

Reinterpretation of the structural evolution of the Broken Hill Inlier through deep seismic reflection profiling and structural mapping has identified a larger component of thrusting, transposition and internal disruption than previously envisaged (Gibson et al., 1998). Seismic images suggest that several of these high temperature shear zones disrupt the Willyama Supergroup to crustal depths of 20–25 km. The new findings are important in order to understand the geometry of the Broken Hill deposit. It was once assumed that the deposit reflected coaxial deformation deduced from unaltered surface outcrop (Hobbs, 1966; Laing et al., 1978). Newer research suggests that deformation was heterogeneous and that fluids were preferentially focussed along shear zones (White et al., 1995; Rothery, 2001). Both the depth and width of the shear zones imply a large potential for fluid movement, especially in the channelling of melt and magmatic fluid during high-temperature metamorphism.

Outcrop mapping to the north of Cannington resulted in two interpretations of the same regional deformation. D_2 (Williams and Phillips, 1992) reflects coaxial deformation, hence large-scale folding, whereas D_4 (Newbery, 1990) resulted in the formation of kilometre-scale shear zones within a fold-and-thrust-belt. D_1 at Cannington closely reflects the description of sigmoidal D_4 fabrics in the vicinity of the Maramungee Zn deposit (Figs. 1 and 14), which is interpreted to lie within the Maramungee Shear Zone (Newbery, 1990). Furthermore, prominent N–S-trending photolinear features that link the Maramungee Zn and Blackrock Zn–Cu–Pb deposits have been interpreted as shear zones (Williams and Heinemann, 1993). Mapping has delineated a common link of shearing at all BHT deposit localities in the area, including the Maramungee Zn, Blackrock Zn–Cu–Pb and Dingo Zn–Cu deposits (Fig. 14). Therefore, similar to a shear zone model at Broken Hill, the SE Mt Isa Inlier can be interpreted to host kilometre-wide thrusts that are spacially related to BHT mineralisation. The Maramungee Shear Zone is interpreted to host the Maramungee Zn and Blackrock Zn–Cu–Pb deposits, and the Dingo Zn–Cu deposit is interpreted to be hosted by the Gidya Tank Shear Zone, which may be within the same thrust duplex as the Maramungee and Levuka Shear Zones of Newbery (1990). Cannington is located to the south of the thrust duplex, although it is slightly offset from the linear trend of the Maramungee Shear Zone. Such an offset may be caused by kilometre-scale displacement along later strike-slip faults that have been described across much of the Mt Isa Inlier (Laing, 1998). Shear zone formation across the width of Cannington, coupled with widths of 0.5–4 km for the Maramungee Shear Zone, suggests that progressive shear zone formation may be responsible for the complete range of asymmetries that have been previously interpreted as having formed by successive folding events (Giles,

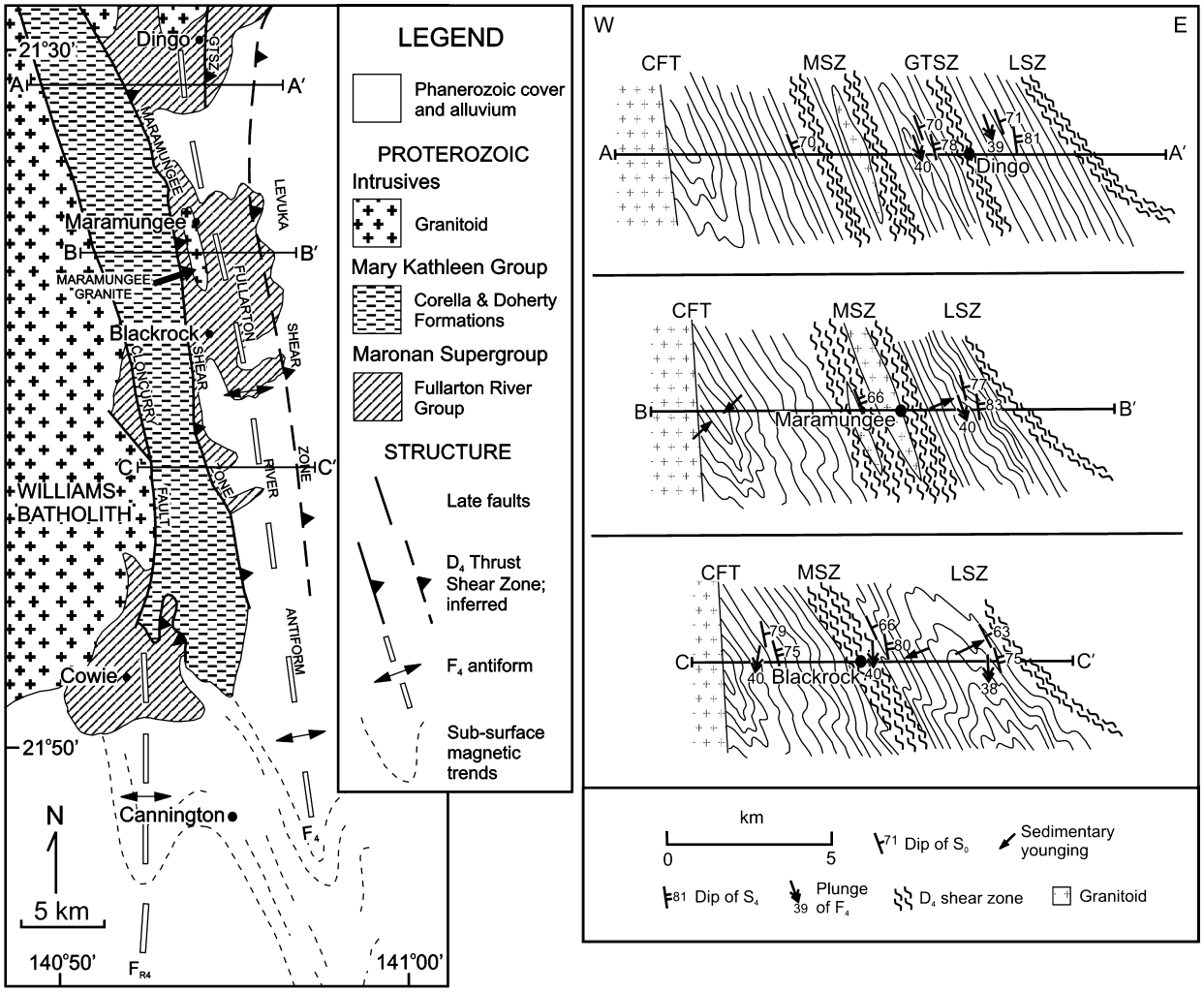

Fig. 14. Cannington in relation to host rocks and structure of the SE Mt Isa Inlier. Outcrop mapping suggests a genetic and spatial correlation between the Maramungee, Levuka and Gidya Tank (GTSZ) Shear Zones and large-scale folding. Dingo, Maramungee and Blackrock base metal deposits are situated within the D_4 (interpreted as D_1 in this study) fold-and-thrust-belt, as is Cannington along an interpreted southerly continuation. Cross-sections through the fold and thrust belt show the affiliation between shear zones and base metal prospects (modified from Newbery (1990)).

2000). Progressive deformation effectively explains the clustering of a particular foliation orientation and/or mineral elongation lineation within a defined area, and is supported by the lack of deformed or cross-cutting lineations (cf. Kamber et al., 1995). Hence, it is interpreted that BHT deposits are situated within shear zones, and are not expected to form within intervening thrust sheets.

The Aggeneys–Gamsberg base metal sulphide deposits of the Namaqualand Metamorphic Complex, South Africa, provide another example of BHT mineralisation within a terrane that has a history of conflicting interpretation. Increasing geological knowledge from structural–stratigraphic mapping and years of developing thrust tectonic theory have resulted in the early polydeformational model (Joubert, 1974) being challenged by a progressive ductile shear model (Colliston et al., 1991). The change from fold to shear models is similar to that of the Broken Hill and Mt Isa Inliers. Nowhere is this more evident than at the Broken Hill deposit, Aggeneys. Discovered in 1971 along with the Black Mountain and Big Syncline deposits, Broken Hill (Aggeneys) was brought into production in 1980 following a comprehensive diamond drilling campaign. The deposit geological model (Ryan et al., 1986) reflected the regional model at the time, and it was not until underground mining exposed a large proportion of the ore body that geological opinion changed to a simpler, shearing origin (Mourant and Smith, 1986). The example of Broken Hill (Aggeneys) also outlines the need for objective data gathering and interpretation, which is often limited when dealing with diamond drill-core.

Description of the structural geology at the Zinkgruvan Zn–Pb–Ag deposit, southern Bergslagen Province, Sweden, places emphasis on large-scale geometries and form surfaces in the interpretation of coaxial folding (Hedstrom et al., 1989). Better documentation of the structure is needed in order to correlate between the two underground workings, but it appears from the literature that a single phase of orogenic deformation was responsible from the description

of small-scale fabrics. The only refolding noted was interpreted to have taken place during post-orogenic granite intrusion. The single phase of orogenic deformation could have resulted from coaxial folding or shearing. Hence, a re-evaluation of the Zinkgruvan geometry could test the shear model presented in this study.

A common pattern of BHT mineralisation affiliated with shear zones, but not with intervening thrust sheets, has been documented in the Broken Hill Inlier, the SE Mt Isa Inlier and the Namaqualand Metamorphic Complex. Potential for extension of this model also exists in the Southern Bergslagen Province, Sweden.

4. BHT exploration in the SE Mt Isa Inlier

Factors that determine the size and location of BHT deposits need to be addressed, particularly to explain why mineralisation at the BHT prospects to the north of Cannington do not reach economic levels. Firstly, the geometry of Cannington is unique in regard to all deposits in the SE Mt Isa Inlier. The Core Amphibolite mega boudin that was shaped by D_1 thrusting may have acted as a structural trap in the concentration of D_2 garnet–pyroxene alteration during extension of S_1. Secondly, the Core Amphibolite proved to be a reactive body for the precipitation of garnet–pyroxene alteration, which is shown through the zoned distribution of hedenbergite and pyroxferroite–pyroxmangite (Chapman and Williams, 1998). Small amphibolite bodies in the footwall of the Core Amphibolite provide a clue as to why economic mineralisation is not found in the prospects to the north of Cannington. These bodies at Cannington are essentially miniature Core Amphibolites, but lack both the size and geometry to enable a sufficient concentration of garnet–pyroxene alteration to create an economic deposit. The Maramungee (Williams and Heinemann, 1993), Dingo and Black Rock (Williams and Phillips, 1992) prospects all contain narrow sheets of amphibolite that have the same features as the small amphibolites at Cannington, but with nothing comparable to the Core Amphibolite.

The Pegmont Pb–Zn prospect west of Cannington (Fig. 1) is hosted by the Kuridala Formation of the Mary Kathleen Group (Derrick et al., 1977), but instead of amphibolite, mineralisation is associated with iron formations (Vaughan and Stanton, 1986). Such a relationship between BHT mineralisation and iron formations is similar to that of the Aggeneys–Gamsberg BHT deposits of South Africa, and the Broken Hill Main Lode, but instead of rheological heterogeneity in the form of an amphibolite body, studies interpret that folding within high-temperature shear zones created low-strain sites that concentrated mineralisation (Mourant and Smith, 1986; Rothery, 2001). The latter interpretation is different to conclusions from this study, in which sulphide lode geometry is dictated by the distribution of garnet–pyroxene alteration and lower temperature deformation. Nevertheless, BHT deposits as a group may not be so different in origin that individual exploration strategies need to be adopted. Shear zones appear to be a common BHT deposit association. Therefore, an understanding of the distribution of shear zones has a central role in determining areas of BHT prospectivity, and lithology may only impact on the style of dilational site within the shear zone.

5. Implications for BHT deposit genesis

The syngenetic argument for BHT deposit genesis has relied in part on the structural interpretation that the deposits are folded. At Cannington, all pre-peak metamorphic mineral fabrics have been obliterated, which reduces the probability of demonstrating a syngenetic origin by structural means, especially as S_1/S_2 has been shown to control the distribution of metasomatic alteration and later sulphide precipitation around the Core Amphibolite. Evidence for a pre-metamorphic deposit includes peak metamorphic sulphide inclusions in garnet, olivine and quartz. These could represent trapped pre-peak metamorphic sulphide (Bodon, 1998), although could equally be late, as garnet in particular is prone to fracturing during retrograde deformation. On the other hand, D_1 gahnite and D_2 quartz inclusions rich in Pb–Zn (Williams et al., 1999) attest to substantial base-metal concentrations in pre-existing sediments. S-poor concentrations within D_2 inclusions, combined with high temperatures during D_2, suggest that the sulphide lodes did not form during D_2, but assumed their current geometry during later cooling. The latter conclusion is supported by the preferential deposition of sulphide upon, and retrogression of, the garnet–pyroxene alteration (Chapman and Williams, 1998).

Similar inclusion chemistry is found in garnet–pyroxene rocks at Broken Hill (Williams et al., 1999), therefore epigenesis most readily accounts for BHT deposit origin, at least in the localised redistribution of sulphide into favoured structural and rheological/chemical sites within shear zones. Indeed, Broken Hill is considered to have undergone multiple stages of mineralisation, as has Cannington with the greatest concentration of mineralisation associated with retrograde shear zone/fault activity (e.g. Trepell Fault). Metasomatic alteration usually obscures early structural evidence, but where it is preserved (e.g. this study) shear zones are seen to control the deposit geometry from early high temperature metasomatism. These factors combine to suggest that even if BHT deposits were of a syngenetic origin, the present geometry is completely controlled by subsequent shear zone deformation and metasomatism. Therefore, even if metal concentrations had existed prior to metamorphism, they have effectively been converted into an upgraded, epigenetic geometry, rather than a less economically attractive or uneconomic precursor.

6. Conclusions

Shear zones and not coaxial folds are responsible for the asymmetries and deposit-scale geometry at Cannington. This is demonstrated by:

1. Consistent senses of asymmetry parallel to L_1 and L_2.
2. A single protracted stage of biotite–sillimanite-muscovite growth during D_2.
3. A synthetic shear sense between passive rotation parallel to S_1, and active folding oblique to S_1.
4. Variation in S_2 orientation that is in response to increasing internal instability with increasing intensity of S_2.
5. Foliated pyroxene–garnet alteration and resistant almandine banding that delineate continuous shear zones at the southern closure of the core amphibolite.
6. Preferential deposition of sulphide upon pyroxene–garnet alteration during a lower-temperature retrograde event.
7. Proto-sheath folding that explains the formation of doubly-plunging F_2.
8. Magmatic flow during folding and rupture of leucosomes, which explains a localised variation in fold shape and attitude.

A revised interpretation of BHT deposits indicates that:

1. Predominantly coaxial fabrics are observed outside altered mine sequences, and non-coaxial fabrics are more common in mine exposure.
2. BHT deposits preferentially occupy sites that are geometrically controlled by high-temperature thrust shear zones and localised rheological and chemical contrast, and are regionally surrounded by mutually synchronous large-scale folding within thrust sheets.
3. Potential areas for ore deposit formation may be duplicated through the formation of thrust duplexes, but only when suitable host rocks are intersected.
4. Even if BHT deposits were originally syngenetic, the present geometry is controlled by subsequent shear zones that transformed marginally economic prospects into viable deposits.

Acknowledgements

This paper is published with the approval of Mick Roche, BHP Billiton Cannington. Thanks to Tom Blenkinsop and Mike Rubenach for helpful discussions. Thanks also go to Eoin Rothery and Ken Maiden for critical comments that led to a great improvement in the content, construct and readability of the paper. The research was conducted whilst the author was a PhD APA(i) scholar as a part of SPIRT grant C00107232.

References

Alsop, G.I., Holdsworth, R.E., 1999. Vergence and facing patterns in large-scale sheath folds. Journal of Structural Geology 21, 1335–1349.

Alsop, G.I., Holdsworth, R.E., 2002. The geometry and kinematics of flow perturbation folds. Tectonophysics 350, 99–125.

Andrews, E.C., 1922. The geology of the Broken Hill district. New South Wales Geological Survey Memoir 8.

Beardsmore, T.J., Newbery, S.P., Laing, W.P., 1988. The Maronan Supergroup: an inferred early volcanosedimentary rift sequence in the Mount Isa Inlier and its implications for ensialic rifting in the Middle Proterozoic of northwest Queensland. Precambrian Research 40/41, 487–507.

Beeson, R., 1990. Broken Hill-type lead-zinc deposits—an overview of their occurrence and geological setting. Transactions of the Institution of Mining and Metallurgy 99, B163–B175.

Bodon, S.B., 1998. Paragenetic relationships and their implications for ore genesis at the Cannington Ag–Pb–Zn Deposit, Mount Isa Inlier, Queensland, Australia. Economic Geology 93, 1463–1488.

Chapman, L.H., Williams, P.J., 1998. Evolution of pyroxene–pyroxenoid–garnet alteration at the Cannington Ag–Pb–Zn Deposit, Cloncurry District, Queensland, Australia. Economic Geology 93, 1390–1405.

Cobbold, P.R., Cosgrove, J.W., Summers, J.M., 1971. Development of internal structures in deformed anisotropic rocks. Tectonophysics 12, 23–53.

Colliston, W.P., Praekelt, H.E., Schoch, A.E., 1991. A progressive ductile shear model for the Proterozoic Aggeneys Terrane, Namaqua mobile belt, South Africa. Precambrian Research 49, 205–215.

Derrick, G.M., Wilson, I.H., Hill, R.M., 1977. Revision of stratigraphic nomenclature in the Precambrian of northwestern Queensland VI: Mary Kathleen Group. Queensland Government Mining Journal 78, 15–23.

Gibson, G., Drummond, B., Fomin, T., Owen, A., Maidment, D., Wake-Dyster, K., 1998. Structural and tectonic evolution of the Broken Hill region revisited: implications for mineral exploration in the Willyama Supergroup. In: Finlayson D.M., Jones L.E.A. (Eds.), Mineral Systems and Crust–Upper Mantle of South-East Australia. Australian Geological Survey Organisation Record 1998/2, pp. 75–77.

Giles, D., 2000. Tectonic setting of Broken Hill-type mineralisation: the Cannington perspective. Ph.D. thesis, Monash University.

Gray, D.R., 1992. Structural report on the Cannington Pb–Zn–Ag deposit, Mount Isa Inlier. Unpublished Report to BHP Minerals.

Gustafson, J.K., Burrell, H.C., Garrety, M.D., 1950. Geology of the Broken Hill ore deposit, Broken Hill, N.S.W., Australia. Geological Society of America Bulletin 61, 1369–1438.

Hedstrom, P., Simeonov, A., Malmstrom, L., 1989. The Zinkgruvan ore deposit, South-central Sweden: a Proterozoic, proximal Zn–Pb–Ag deposit in distal volcanic facies. Economic Geology 84, 1235–1261.

Hobbs, B.E., 1966. The structural environment of the northern part of the Broken Hill orebody. Journal of the Geological Society of Australia 13, 315–338.

Jeffrey, S., 2002. The Cannington Ag–Pb–Zn BHT deposit; a world class discovery with a silver lining. In: Preiss, V.P. (Ed.), Geoscience 2002: Expanding Horizons. Abstracts of the 16th Australian Geological Convention, Adelaide Convention Centre, Adelaide, SA, Australia, July 1–5 2002, 67, p. 265.

Joubert, P., 1974. The gneisses of Namaqualand and their deformation. Transactions of the Geological Society of South Africa 77, 339–345.

Kamber, B.S., Blenkinsop, T.G., Villa, I.M., Dahl, P.S., 1995. Proterozoic transpressive deformation in the Northern Marginal Zone, Limpopo Belt, Zimbabwe. The Journal of Geology 103, 493–508.

Laing, W.P., 1998. Structural–metasomatic environment of the East Mt Isa

Block base-metal–gold province. Australian Journal of Earth Sciences 45, 413–428.

Laing, W.P., Marjoribanks, R.W., Rutland, R.W.R., 1978. Structure of the Broken Hill mine area and its significance for the genesis of the orebodies. Economic Geology 73, 1112–1136.

McLellan, E.L., 1984. Deformational behaviour of migmatites and problems of structural analysis in migmatite terranes. Geological Magazine 121, 339–345.

McLellan, E.L., 1988. Migmatite structures in the Central Gneiss Complex, Boca de Quadra, Alaska. Journal of Metamorphic Geology 6, 517–542.

Mark, G., Phillips, G.N., Pollard, P.J., 1998. Highly selective partial melting of pelitic gneiss at Cannington, Cloncurry District, Queensland. Australian Journal of Earth Sciences 45, 169–176.

Mourant, D., Smith, P., 1986. Addendum to the paper by Ryan et al. (1986) on the Aggeneys base metal sulphide deposits, Namaqualand District. In: Anhaeusser, C.R., Maske, S. (Eds.), Mineral Deposits of Southern Africa, Geological Society of South Africa, Johannesburg, p. 1475.

Newbery, S.P., 1990. The middle Proterozoic Maranoan Supergroup, Soldiers Cap Belt, Eastern Mount Isa Inlier; a rationalization of the geology and mineralization of a complexly deformed and metamorphosed terrane. Ph.D. thesis, James Cook University.

Page, R.W., Sun, S.-s., 1998. Aspects of geochronology and crustal evolution in the Eastern Fold Belt, Mt Isa Inlier. Australian Journal of Earth Sciences 45, 343–361.

Parr, J.M., Plimer, I.R., 1993. Models for Broken Hill-type lead–zinc–silver deposits. In: Kirkham, R.V., Sinclair, W.D., Thorpe, R.I., Duke, J.M. (Eds.), Mineral Deposit Modelling. Geological Association of Canada, Special Paper 40, pp. 253–288.

Passchier, C.W., Trouw, R.A.J., Zwart, H.J., Vissers, R.L.M., 1992. Porphyroblast rotation: eppur si mouve? Journal of Metamorphic Geology 10, 283–294.

Ramsay, J.G., Graham, R.H., 1970. Strain variation in shear belts. Canadian Journal of Earth Sciences 7, 786–813.

Richmond, J.M., Chapman, L.H., Williams, P.J., 1996. Two phases of garnet growth at the Cannington Ag–Pb–Zn deposit, NW Queensland. In: Baker, T., Rotherham, J., Richmond, J., Mark, G., Williams, P. (Eds.), New Developments in Metallogenic Research: The McArthur, Mt Isa, Cloncurry Minerals Province. James Cook University of North Queensland Economic Research Unit Contribution 55, pp. 113–117.

Rothery, E., 2001. Tectonic origin of the shape of the Broken Hill lodes supported by their structural setting in a high-grade shear zone. Australian Journal of Earth Sciences 48, 201–220.

Ryan, P.J., Lawrence, A.L., Lipson, R.D., Moore, J.M., Paterson, A., Stedman, D.P., Van Zyl, D., 1986. The Aggeneys base metal sulphide deposits, Namaqualand District. In: Anhaeusser, C.R., Maske, S. (Eds.), Mineral Deposits of Southern Africa, Geological Society of South Africa, Johannesburg, pp. 1447–1473.

Sheehan, P., 1994. The structural geology of the host rocks to the Ag–Pb–Zn mineralisation at BHPs Cannington Deposit, Eastern Fold Belt, NW Queensland. Honours thesis, Monash University.

Vaughan, J.P., Stanton, R.L., 1986. Sedimentary and metamorphic factors in the development of the Pegmont stratiform Pb–Zn deposit, Queensland. Transactions of the Institute of Mining and Metallurgy 95, B94–B121.

Walters, S.G., 1998. Broken Hill-type deposits. AGSO Journal of Australian Geology & Geophysics 17, 229–237.

Walters, S.G., Bailey, A., 1998. Geology and mineralisation of the Cannington Ag–Pb–Zn deposit: an example of Broken Hill-type mineralisation in the Eastern Succession, Mount Isa Inlier, Australia. Economic Geology 93, 1307–1329.

White, S.H., Rothery, E., Lips, A.W., Barclay, T.J.R.B., 1995. Broken Hill base-metal deposit: a tectonically transported and modified basinal deposit within the Proterozoic Willyama Fold and Thrust Belt. Transactions of the Institution of Mining and Metallurgy 104, B1–B17.

Williams, P.J., Heinemann, M., 1993. Maramungee: a Proterozoic Zn skarn in the Cloncurry District, Mount Isa Inlier, Queensland, Australia. Economic Geology 88, 1114–1134.

Williams, P.J., Phillips, G.N., 1992. Cloncurry mapping project 1990: Geology of the Selwyn Range (McKinlay River and Maramungee Creek areas). James Cook University Economic Geology Research Unit Contribution 40.

Williams, P.J., Guoyi, D., Prendergast, K., Pollard, P.J., Ryan, C.G., 1999. Metasomatism and metal mobility in Broken Hill-type deposits. In: Stanley, C.J., et al. (Eds.), Proceedings of the Fifth Biennial SGA Meeting and the Tenth Quadrennial IAGOD Meeting, London, UK, pp. 999–1002.